Initial Performance of a ECR Waveguide Plasma Cathode with Permanent Magnets

IEPC-2009-211

Presented at the 31st International Electric Propulsion Conference,
University of Michigan • Ann Arbor, Michigan • USA
September 20 – 24, 2009

Brandon R. Weatherford[1] and John E. Foster[2]
University of Michigan, Ann Arbor, MI, 48104, USA

Abstract: The design and initial characterization of the U-M ECR waveguide plasma cathode is presented. The source was tested at currents up to 1.7 A, the upper limit of the power supply used in this investigation. Characterization of the extracted electron current sensitivity to orifice size and flow revealed a monotonic increase in performance with decreasing orifice size. Electron production and extraction efficiencies of as low as 115 W/A were measured on this unoptimized source. Performance gain due to significant ion recycling was documented with effective gas utilization of nearly 800 percent.

Nomenclature

a	=	waveguide radius
$a_{c,nm}$	=	cutoff radius for TE_{nm} or TM_{nm} mode
A_{ori}	=	area of extraction orifice
c	=	speed of light in vacuum
e	=	elementary charge
ε	=	permittivity
f	=	microwave frequency
J_n	=	n^{th} Bessel function of the first kind
J_n'	=	derivative of n^{th} Bessel function of the first kind
k	=	Boltzmann constant
k_c	=	cutoff wave number
k_z	=	axial wave number
k_0	=	free space wave number
λ_g	=	guide wavelength
m	=	electron mass
μ	=	permeability
n	=	plasma density
p_{nm}	=	m^{th} root of J_n
p'_{nm}	=	m^{th} root of J_n'
T_e	=	electron temperature
ω	=	microwave frequency
ω_c	=	electron cyclotron frequency

[1] Graduate Student, Department of Nuclear Engineering and Radiological Sciences, brweathe@umich.edu
[2] Associate Professor, Department of Nuclear Engineering and Radiological Sciences, jefoster@umich.edu

I. Introduction

THE hollow cathode assembly (HCA) is an established technology which has been utilized as an electron source in electric propulsion (EP) systems, both as the primary discharge cathode and ion beam neutralizer dating back to the 1960s.[1] Although the legacy and high performance of the hollow cathode makes it an attractive option for many applications, the lifetime of the HCA is limited by several failure mechanisms. The primary failure mechanism of hollow cathodes is the depletion of work function lowering impregnate due to either evaporation or thermochemical conversion of impregnate to inert compounds.[2,3] Additionally, erosion of the cathode's orifice and orifice plate, as well as the keeper assembly, can lead to premature failure.[3] These failure mechanisms occur over an extended period of time. Based on recent wear testing, the lifetime for a conventional HCA is estimated to be approximately 36,000 hours.[3] For those missions requiring operational times significantly longer than this, such as those involving robotic probes to the outer planets, total thruster operational times will greatly exceed 36,000 hours; therefore, the investigation of new technologies that can circumvent this limitation is warranted. These newer technologies include reservoir cathodes, LaB_6 cathodes, carbon composition cathodes, and electrodeless plasma cathodes.[4-7] Here, by plasma cathodes, we refer to those systems that extract electrons from a dense plasma source.[8]

As demonstrated in the HAYABUSA mission, a microwave plasma discharge can be employed as the primary ionizer for the production of ions as well as the electron source for beam neutralization in an ion thruster without the need for thermionic emitters.[9] The μ10 neutralizers on HAYABUSA featured a plasma cathode in which an electron cyclotron resonance plasma was produced by a wire antenna.[10] While this approach completely eliminates the problem of the depletion of emissive material in HCAs, the exciting antenna is in direct contact with plasma and is therefore still vulnerable to erosion through ion bombardment. Indeed, the lifetime of such a plasma cathode is limited by such erosion.[11]

There have been several varieties of microwave plasma cathodes that have been investigated for electric propulsion applications. One embodiment uses the intense microwave electric field in a resonant cavity to produce the plasma.[12] The more conventional approach is to exploit electron cyclotron resonance (ECR). In ECR, electrons can gain energy by the resonant absorption of the incident microwaves.[10,13,14] Helicon plasma cathodes also involve the resonant absorption of electromagnetic radiation, albeit at lower frequencies, by electrons. Helicon sources are attractive because of the relatively high plasma densities attainable using the helicon resonant absorption. The Non-ambipolar Electron Source employs a high-power helicon plasma as the electron source.[15]

Although aforementioned approaches have been able to deliver electron current without the use of a thermionic emitter, no serious investigations of a low-to-medium power microwave plasma cathode using permanent magnets have been able to deliver the required currents for ion beam neutralization while avoiding the erosion problem that arises from the use of a launching antenna in contact with the discharge. Such a source would also have an advantage over helicon sources, in that it would eliminate the need for the use of a fragile dielectric cavity or heavy electromagnets. The goal of this paper is to present the design and initial performance of an ECR waveguide plasma cathode that is being developed at the U-M Plasma Science and Technology Laboratory for EP applications. The plasma source employs permanent magnets to set up a predominantly axial-magnetic field, used for plasma confinement and to set up the required conditions for ECR heating by 2.45 GHz microwaves. The source avoids any possibility of erosion because rather than using an antenna to launch the microwaves, a traveling wave is used instead to heat the discharge. The basic reasoning behind the source design is presented, along with some modeling results. The performance of the source was inferred from measured extracted current magnitude as a function of extraction voltage for several different extraction apertures, all as a function of absorbed microwave power and gas flow rate. Langmuir probe data was also acquired near the exit plane of the source to give some insight into the operation of the source. Based on the trends observed during testing, future steps toward optimizing and understanding the source operation are identified.

II. Device Design Basis

The waveguide ECR plasma cathode was developed as an improved version of previous efforts to develop a similar source at the University of Michigan.[16] There were two main areas of focus to consider when designing such a source – the microwave circuit and the magnetic field configuration.

Because the device employs traveling microwaves as the discharge heating source, the source geometry has inherent size constraints which are related to propagation cutoff in the waveguide and microwave mode competition. As this source design is based on a circular waveguide, it is possible to determine the ideal waveguide dimensions for meeting both of these conditions. For each possible TE_{nm} waveguide mode, a cutoff radius can be assigned, given by,

$$a_{c,nm} = \frac{p'_{nm}}{2\pi f\sqrt{\mu\varepsilon}} \tag{1}$$

where $a_{c,nm}$ is the cutoff radius for mode TE_{nm}, f is the microwave frequency, μ and ε are the permeability and permittivity, respectively, of the medium within the waveguide, p'_{nm} is the m^{th} root of J_n', and J_n' is the derivative of the n^{th} Bessel function of the first kind. Similarly, for each TM_{nm} mode, the cutoff radius is,

$$a_{c,nm} = \frac{p_{nm}}{2\pi f\sqrt{\mu\varepsilon}} \tag{2}$$

where p_{nm} is the m^{th} root of J_n, and J_n is just the n^{th} Bessel function of the first kind. In a circular waveguide, the lowest-order propagation mode is the TE_{11} mode, so ideally, the source design should have a waveguide radius larger than the cutoff radius for the TE_{11} mode, but smaller than the cutoff radius for all other modes. This will allow for the TE_{11} mode to propagate in the waveguide without attenuation, while eliminating any mode competition from higher-order modes. While it would also be possible to design a source that runs in the TM_{01} mode, such a source would have to be slightly larger than the TE_{11} source. The TE_{11} mode is peaked on axis, and because of the magnetic circuit geometry to be used, it is a better-suited mechanism for launching the right-hand circularly polarized wave necessary for ECR heating than the TM_{01} mode.

The ECR waveguide plasma source described herein uses 2.45 GHz microwaves. By Eq. (1), it follows that at this frequency, the cutoff radius for the circular TE_{11} mode is 3.59 cm. Equation (2) gives a cutoff radius of 4.69 cm for the TM_{01} mode, and the cutoff radii for all other modes are larger than either of these values. The most suitable waveguide radius is then some value between 3.59 cm and 4.69 cm. Based on these calculations, the waveguide radius of the actual source was set at 3.8 cm, to keep the source as small as possible while ensuring that the TE_{11} mode would not be cut off.

The waveguide source length was determined by the guide wavelength of 2.45 GHz microwaves in a 3.8 cm radius waveguide. The source was designed with the assumption that the end of the waveguide would be terminated by a plate with a small orifice, which is assumed to act as a waveguide short. The guide wavelength λ_g is given by,

$$\lambda_g = 2\pi / k_z \tag{3}$$

where k_z is the axial wave number, given by,

$$k_z = \sqrt{k_0^2 - k_c^2} \tag{4}$$

k_c is the cutoff wave number for the TE_{11} mode, given by,

$$k_c = 1.841 / a \tag{5}$$

k_0 is the free space wave number, given by,

$$k_0 = \omega / c \tag{6}$$

$\omega = 2\pi f$, a is the waveguide radius, c is the speed of light in vacuum, and f is the microwave frequency in Hz.

The length of the source was chosen such that the distance between the pressure window and the end terminating orifice plate was larger than a quarter of a wavelength to assure maximum field within the source. Once the waveguide inner dimensions were chosen, the magnetic circuit was designed using the Ansoft Maxwell 2D and Maxwell 11 software packages. Having a waveguide diameter as small as possible allowed for the construction of a permanent magnet configuration that sets up the required field for ECR heating on the waveguide axis. The electron cyclotron resonance condition is met when the electron cyclotron frequency is equal to the angular microwave frequency, that is,

$$\omega = \omega_c \tag{7}$$

where ω is the microwave angular frequency and ω_c is the electron cyclotron frequency. For 2.45 GHz microwaves, the magnetic field strength required to satisfy Eq. (7) is 875 Gauss. Pure ECR heating takes place when the 875 Gauss magnetic field is oriented parallel to the microwave propagation vector and perpendicular to the microwave electric field. Therefore, the goal of the magnetic circuit design was to determine the ideal SmCo magnet geometry to set up an axial, 875 Gauss magnetic field in as large a volume as possible. Ideally, this resonant heating zone would be located on the axis of the waveguide, because the circular TE_{11} mode has an electric field which is peaked on axis.

The final design of the magnetic circuit is shown in Fig. 1. The resonance zone is set up by two rings of SmCo magnets, arranged around the outside of the waveguide, and oriented axially. It is clear that the green resonance heating zone is spread throughout the region within the magnet rings, and is mostly oriented along the waveguide axis. The axial magnetic field has the additional benefit of allowing electrons produced in the heating zone to easily stream along the field lines to the exit plane of the source, while confining electrons from the walls of the source near the magnet rings.

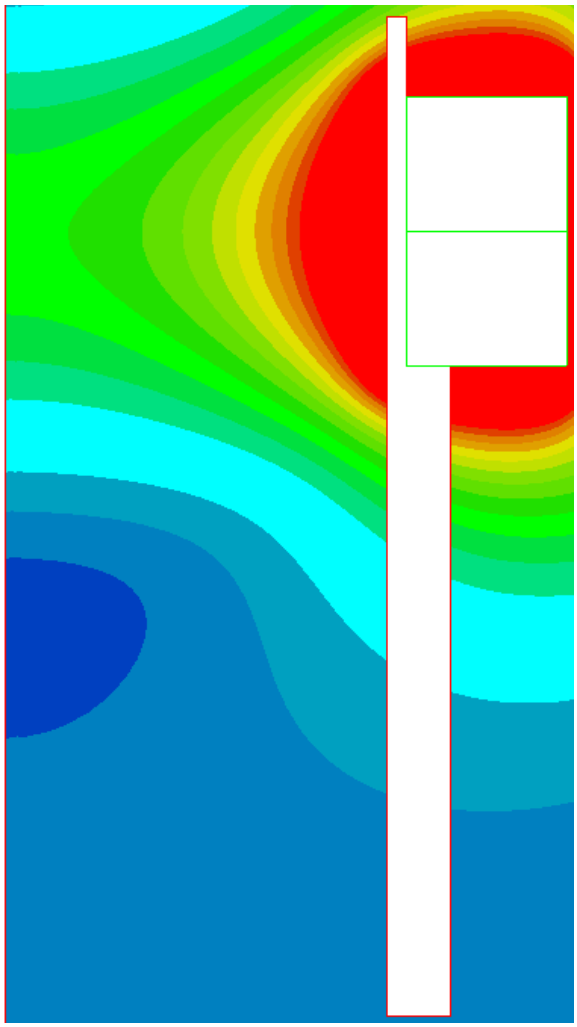

Figure 1. Contour plot of magnetic field strength within waveguide. Leftmost edge is waveguide axis. ECR heating zone shown in bright green.

III. Experimental Setup

A. Device Description

A schematic of the U-M waveguide plasma cathode is shown in Fig. 2. The device consists of a section of cylindrical waveguide, silver soldered to two brass flanges. The waveguide section is necked near the top flange, forming a groove where samarium cobalt magnets are arranged, all oriented parallel to the waveguide axis. The top flange of the source has an O-ring groove, where a quartz pressure window seals the source. The bottom flange seals against a Teflon washer for electrical isolation.

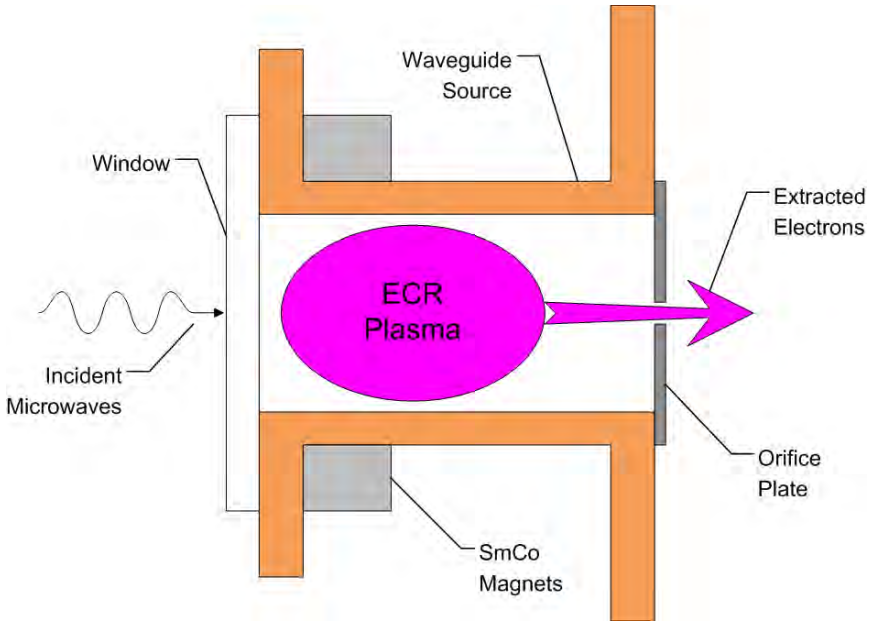

Figure 2. Sketch of the waveguide plasma cathode.

B. Testing Facility

The plasma source was mounted to the top of a stainless steel vacuum chamber, with length 62 cm and inner diameter 42 cm. The source is isolated from the chamber by the Teflon washer, sealed on either side with Viton O-rings. The source exhausts into the vacuum chamber, which is evacuated with a Pfeiffer-Balzers TPU 170 turbomolecular pump, backed by a Pfeiffer L 80 rotary vane pump. Argon gas is fed into the source through a 3.2 mm stainless steel plenum ring located near the pressure window. The gas flow is controlled by a Vacoa MV-25 metering valve, and measured by an Omega FMA 1802 flow meter. The chamber pressure is directly monitored by a Lesker KJL-6000 thermocouple and G100F ion gauge. There is no a direct measurement of the gas pressure within the source itself. A photograph of the testing facility is shown in Fig. 3.

The 2.45 GHz microwaves were generated by a magnetron. Reflected power was managed using a 3-port circulator. Forward and reflected power was measured using a two port directional couple with 60 dB attenuation in conjunction with two power meters. A three stub tuner was used to minimize reflected power. A rectangular to circular waveguide transition was used to couple the power to the circular plasma cathode. The waveguide transition was electrically isolated from the waveguide source by a thin mica washer and the pressure window. A high power microwave cable is used to transmit microwaves from the magnetron assembly to the waveguide transition/plasma source assembly. A photograph of the microwave circuit is shown in Fig. 4.

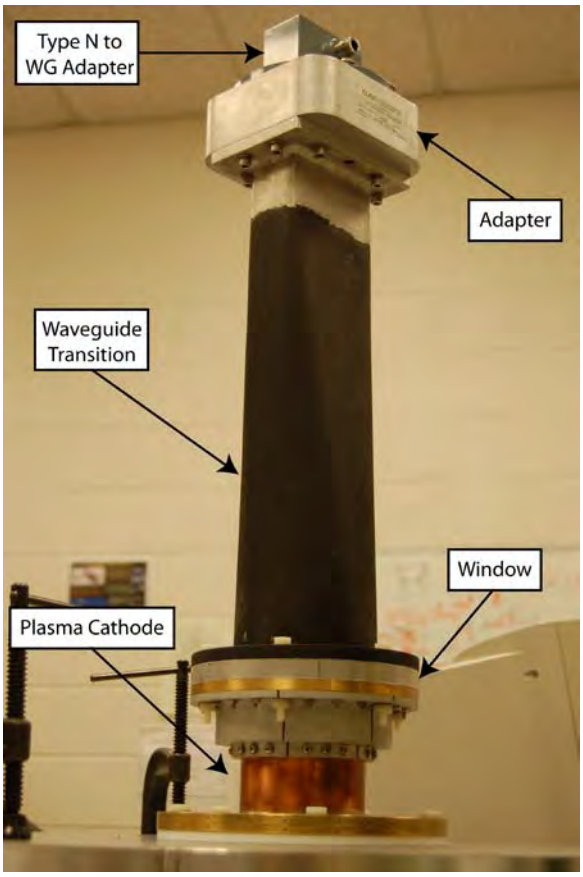

Figure 3. Photograph of the plasma source and testing facility.

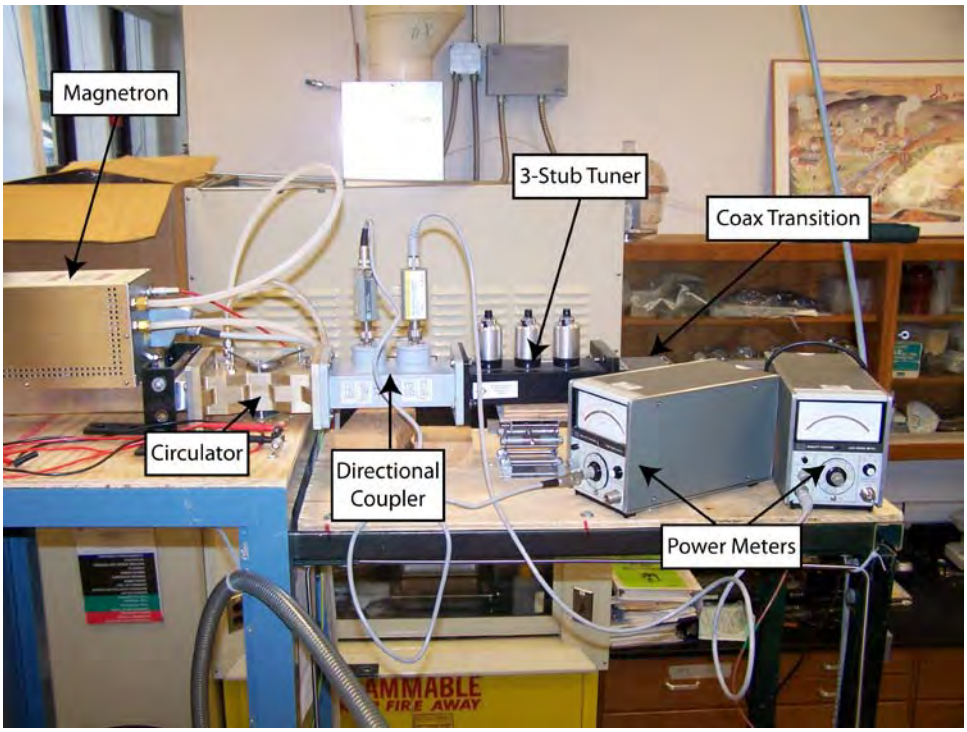

Figure 4. Photograph of the microwave setup.

C. Diagnostics

Two basic diagnostics were employed in this study. A 12 cm diameter molybdenum extraction electrode was installed in the vacuum chamber, on axis, 14 cm downstream of the waveguide plasma source. The electrode was isolated from the vacuum chamber walls, and biased relative to the waveguide source walls using a 600 V, 1.5 A DC power supply. The extracted current and applied voltages were measured with two precision multimeters. A schematic of the current extraction circuit is shown in Fig. 5.

A cylindrical Langmuir probe was used to determine the plasma density and electron temperature within the source at optimized operating points. The molybdenum probe wire tip had a diameter of .508 mm and length of 6 mm. The probe voltage and corresponding current were swept and recorded automatically using an automated data acquisition system connected to a PC. The probe was oriented parallel to the waveguide axis, and the probe tip was located 10 mm from the orifice plate, offset roughly 11 mm from the center of the orifice.

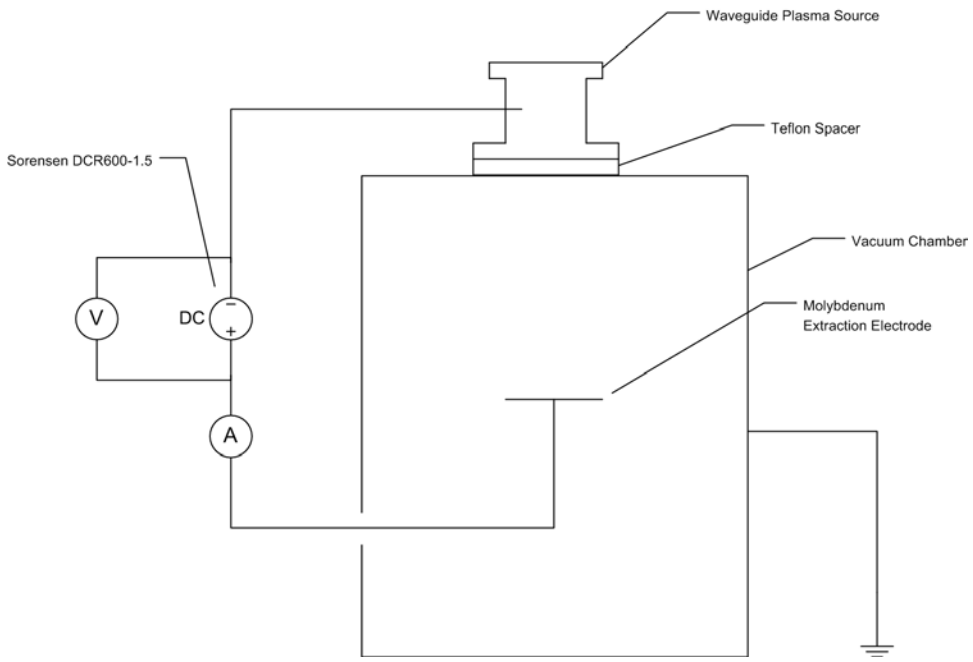

Figure 5. Schematic of electron current extraction circuit.

IV. Experimental Results

A. Orifice Comparison Study

The first series of tests involved determining the electron extraction sensitivity to changes in extraction orifice size, including no orifice plate at all, as a function of power, voltage and flow rate. Unterminated electron extraction (without an orifice plate), was measured as a function of argon flow rate and absorbed microwave power, for a fixed electrode bias of 100 Volts. The results are shown in Fig. 6.

The maximum extractable current from the open source with 100 Volt extraction bias was 0.52 A, at an Ar flow rate of 8 sccm and absorbed microwave power level of 120 W. It is clear from Fig. 6 that the current increases with absorbed microwave power, as expected, however at power levels above 80 W, there appears to be diminishing returns on the amount of additional current from supplying more power. Saturation of current with increasing power above 80 W is likely a consequence of poor neutral confinement in the unterminated case. As power is increased, at a given flow rate/pressure in the source, the ionization fraction is maximized presumably around 80 W. At higher powers, the ionization fraction cannot significantly increase at that pressure because the ionization probability is pressure limited. This is consistent with the increase in current with flow at a given power level. In short, the pressure is simply too low for the density to increase appreciably with increasing power beyond 80 W. The source continues to deliver more current at higher flow rates. Since a flow rate of 8 sccm is somewhat high relative to the extracted electron current, the next goal was to reduce the gas flow rate required for a given extracted current. One way to do this is to reduce the flow conductance between the waveguide source and the exhaust chamber by terminating the waveguide source with an extraction orifice. Such an orifice would increase the operating pressure within the source for a fixed flow rate, ideally improving the source performance.

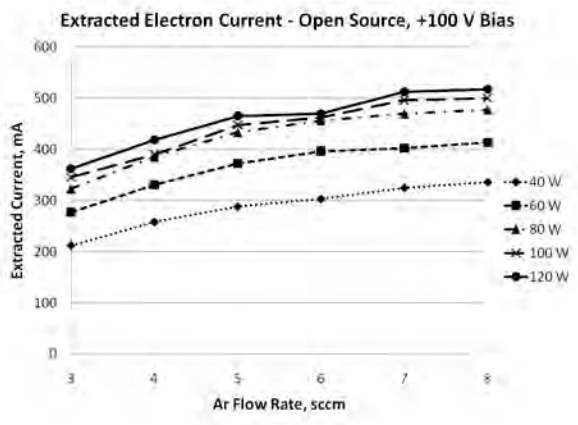

Figure 6. Extracted current vs. absorbed power, flow rate at 100 V.

To obtain a rough mapping of the source's sensitivity to varying pressure, four orifice plates of different orifice area were tested. Each orifice plate was made of steel sheet metal, each of which were mounted to the source using an indium gasket at the interface, which provided enhanced electrical conductivity between the orifice plate and waveguide walls. The orifice plates tested had circular openings of diameters 19 mm, 13 mm, 6.5 mm, and 4 mm.

The extracted current from the 19 mm orifice is shown in Fig. 7 for three electrode bias voltages: 60 V, 80 V, and 100 V. As expected, the amount of current increases both with absorbed power and extraction voltage. In addition, the current increases monotonically with gas flow rate, suggesting that ionization rate increases with gas flow/pressure. As observed in the unterminated case, at powers above 80 W, the current increases more rapidly with power than it does at powers below 80 W. This behavior suggests that pressure must be increased to obtain the benefits of higher power operation. The highest measured current from the 19 mm orifice configuration was 0.9 A, at 6 sccm, 80 W, and with 100 V applied to the extraction electrode. At 100 V, the behavior of the extracted current with flow was essentially linear in contrast to the nonlinear behavior at the lower bias voltages.

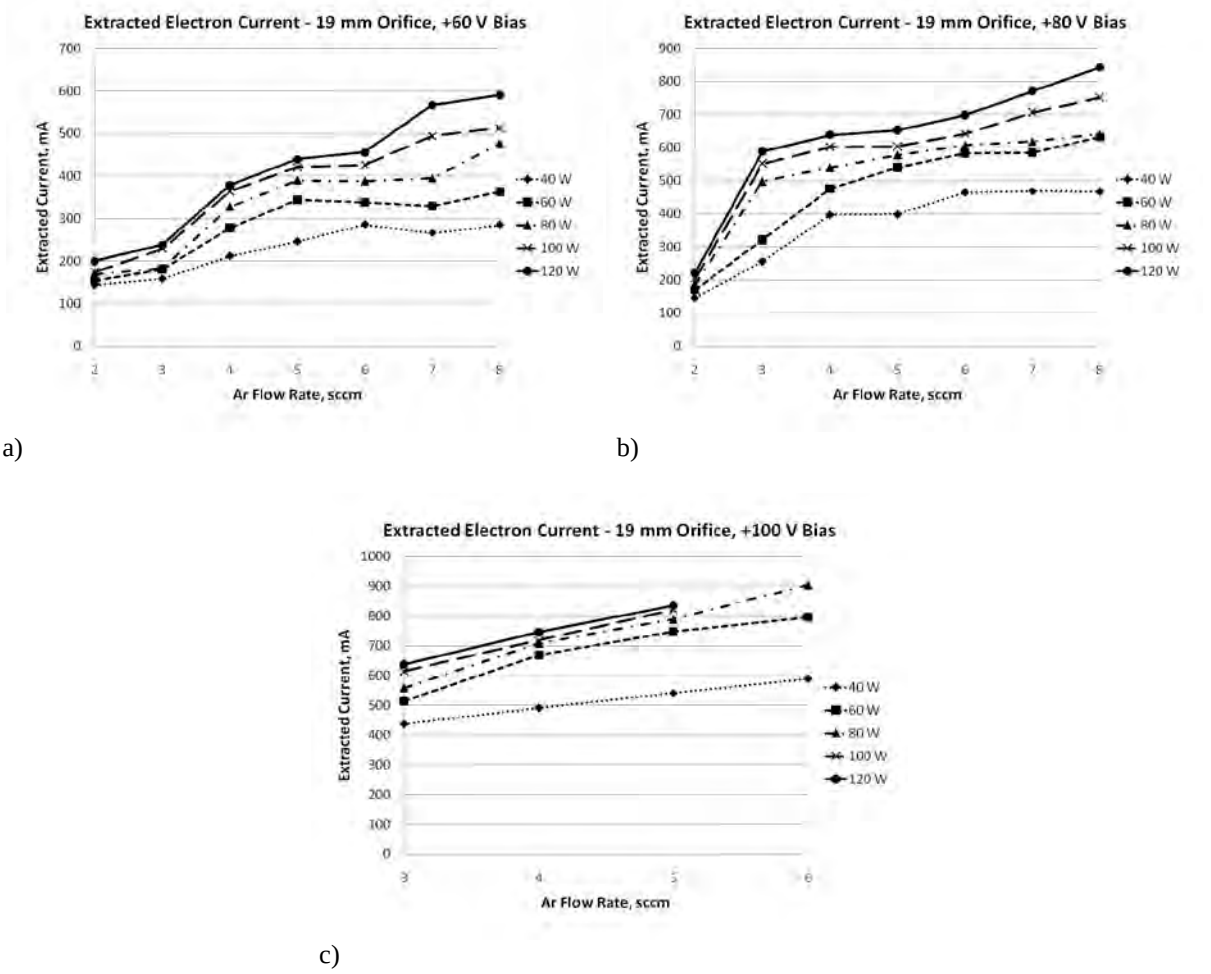

Figure 7. Extracted electron currents versus microwave power and flow rate, for 19 mm extraction orifice, and electrode bias of: a) 60 V, b) 80 V, and c) 100 V.

The orifice area was then roughly halved by operating with a 13 mm orifice. The extractable current was measured in the fashion described previously. The resulting plots of electron current versus flow rate and absorbed power are shown in Fig. 8. Again, the current increased with absorbed power, increasing flow rate and extraction voltage. Overall, at a given flow, microwave power, and extraction voltage, the 13 mm orifice performed better than the 19 mm orifice, producing 1.38 A rather than .90 A, at 6 sccm 80 W, and 100 V. The data appear to suggest that performance improvements with the smaller orifice increase with bias voltage; that is, the difference between the 13 and 19 mm orifice cases are most dramatic at the highest extraction voltage, 100 V. The maximum current extracted from this configuration was 1.44 A, at 5 sccm, 120 W absorbed power, and 100 V bias. Because the current level

continued to increase at higher flow rates, the next phase of testing was with a smaller orifice, to increase the operating pressure further, but at lower input flow rates.

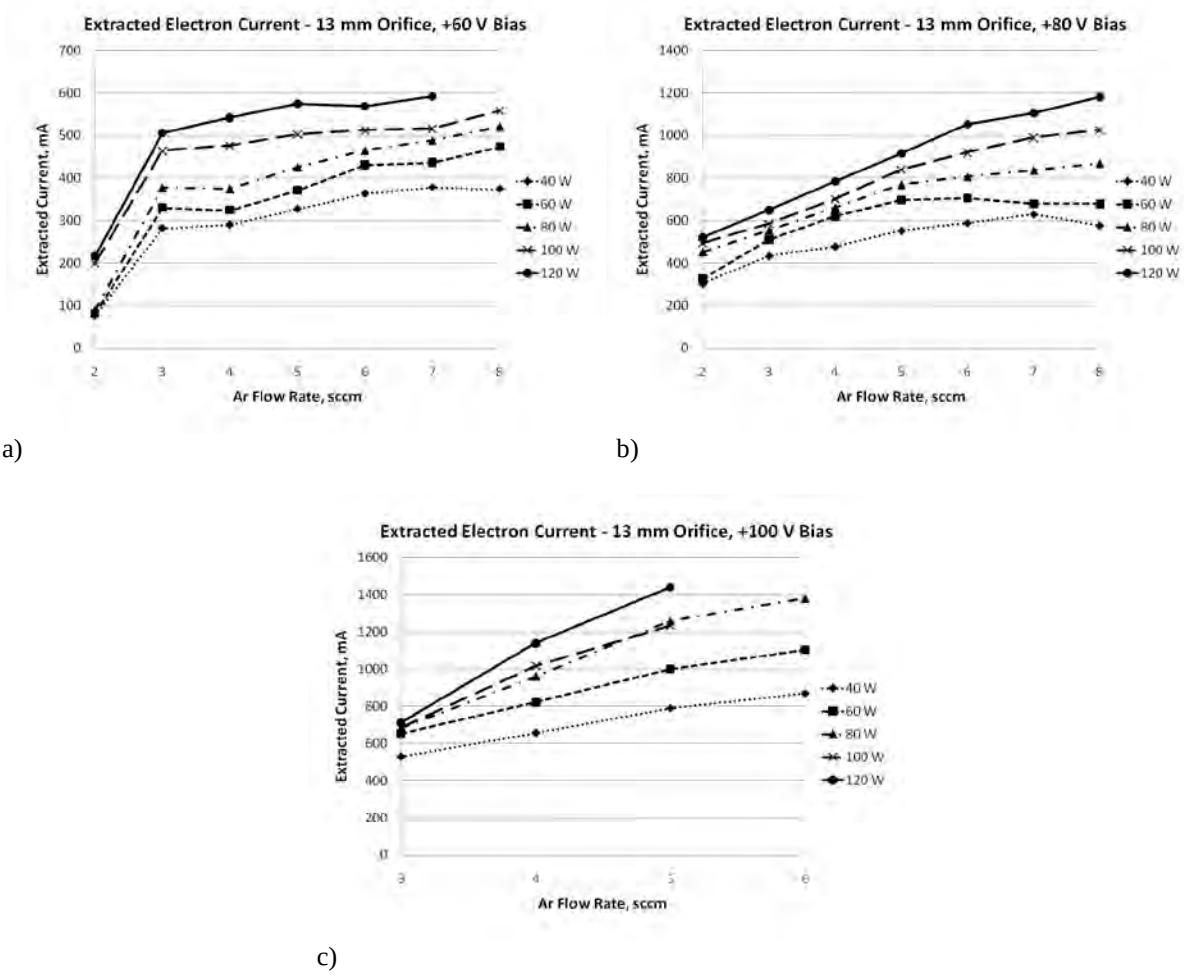

Figure 8. Extracted electron currents versus microwave power and flow rate, for 13 mm extraction orifice, and electrode bias of: a) 60 V, b) 80 V, and c) 100 V.

The 6 mm diameter orifice was installed, constituting a factor of four reduction in area. Extraction results are shown in Fig. 9. The same trends in current with respect to flow rate, power, and extraction voltage continued with the 6 mm orifice. Interestingly though, the curves' slopes tended to increase, becoming more steep with the smaller orifice, making this orifice a better performer than the 13 mm case. However, in the 100 V extraction case, the current capacity of the power supply was reached, at 1.7 A, for two different operating conditions. The 1.7 A mark was reached at 5 sccm, 120 W, and also at 7 sccm, 100 W. Particularly in the 60 V and 80 V extraction cases, higher flow rates continued to provide higher currents. Although it would not be possible to extract over 1.7 A because of the power supply limitations, it was worthwhile to perform an additional test with an even smaller orifice, to determine whether comparable current levels could be achieved at still lower flow rates and power levels.

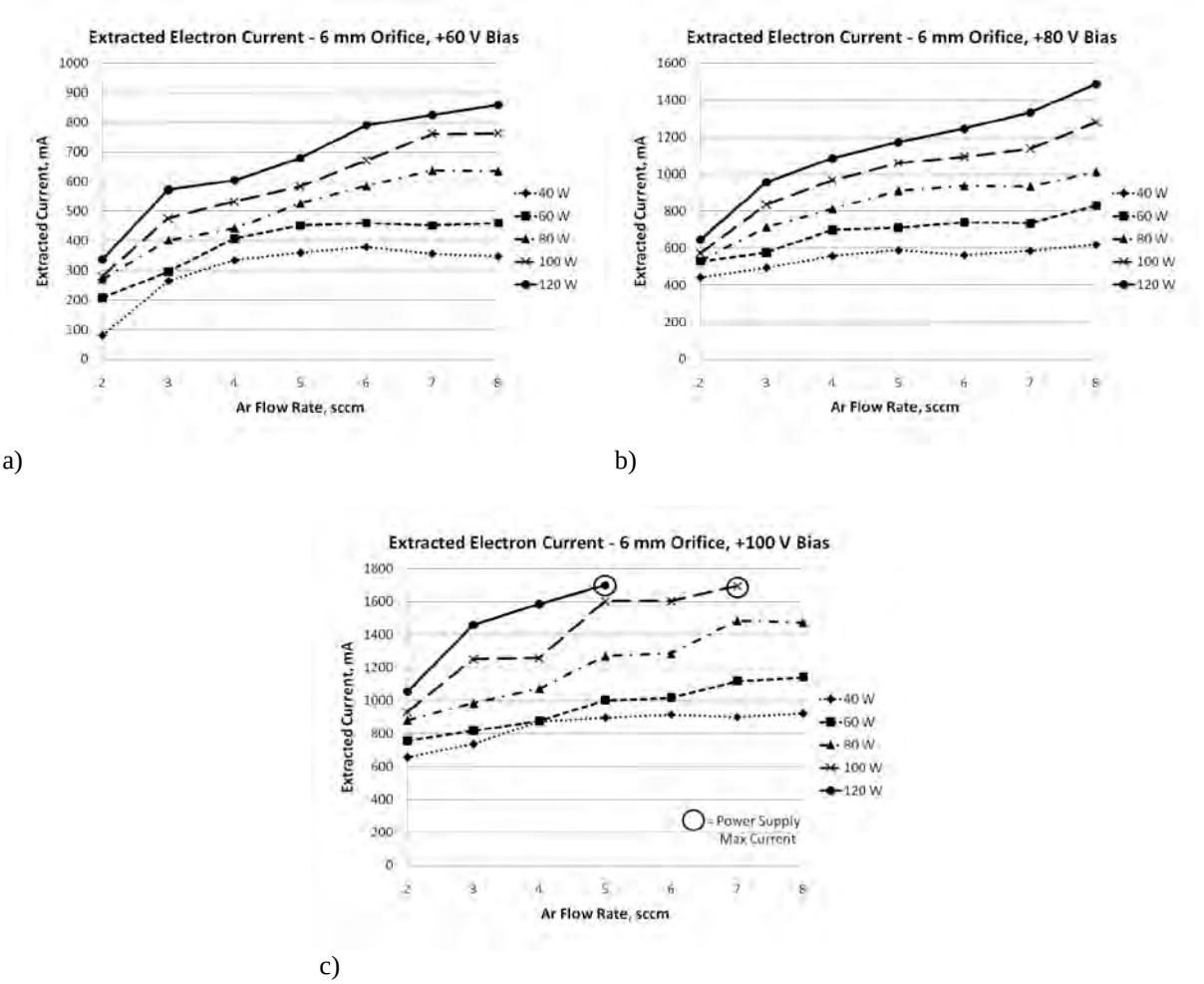

Figure 9. Extracted electron currents versus microwave power and flow rate, for 6 mm extraction orifice, and electrode bias of: a) 60 V, b) 80 V, and c) 100 V.

The final orifice tested was 4 mm in diameter, a roughly twofold decrease in extraction area. Again, the extracted current was measured at 60, 80, and 100 V bias. For a given flow rate, testing was stopped when the 1.7 A maximum current was reached, and then the next flow rate was tested. A photograph of the source running with the 4 mm orifice is shown in Figure 10, and the results from this configuration are shown in Fig. 11. The performance of the source was by far the best with the 4 mm orifice. The power supply-limited current of 1.7 A was achieved at 80 Volts at three different operating conditions, and at 100 Volts at four operating conditions. The 1.7 A current could be extracted at microwave power levels as low as 60 W, or flow rates as low as 3 sccm, depending on the other conditions.

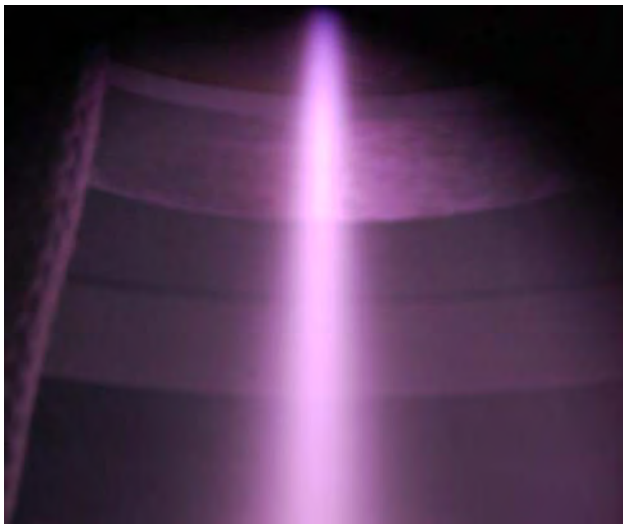

Figure 10. Plasma plume emanating from the extraction orifice of the plasma source (top).

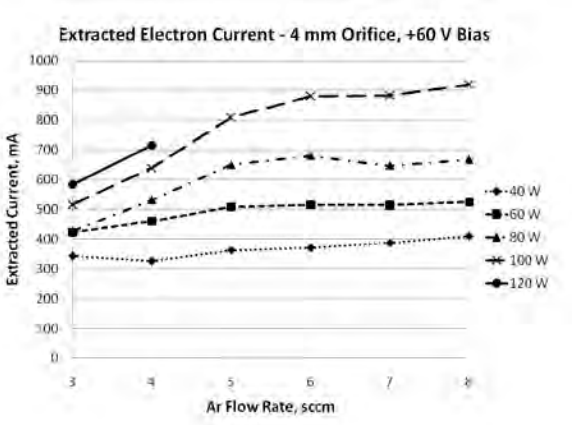

a)

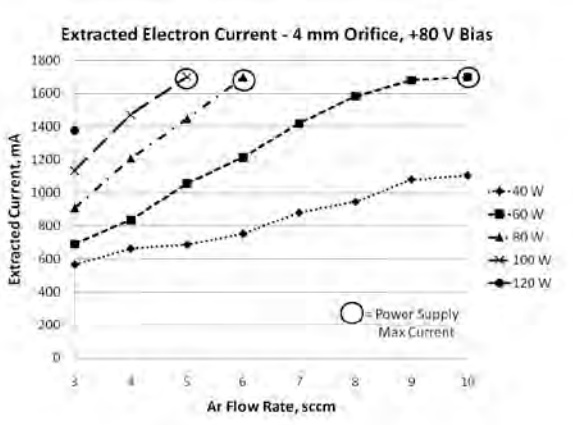

b)

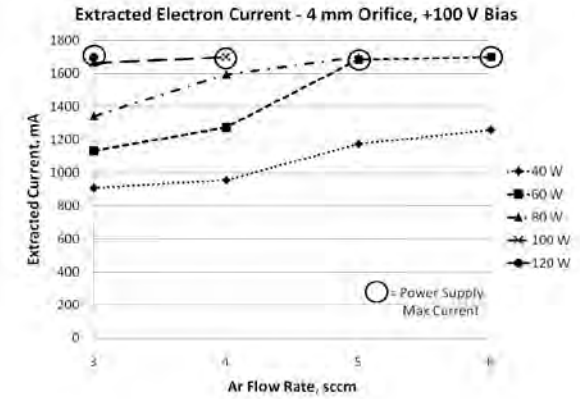

c)

Figure 11. Extracted electron currents versus microwave power and flow rate, for 4 mm extraction orifice, and electrode bias of: a) 60 V, b) 80 V, and c) 100 V.

B. **Power Consumption and Gas Utilization**

A useful performance measure is the total power consumption per ampere of extracted current. The total power consumed is defined as heating power plus the power consumed in the beam extraction circuit. The total power cost at 100 V for the 4 mm orifice is shown in Fig. 12, which gives values between 131 and 171 W/A. It is worth noting that the minimum total power consumption, 115 W/A, was achieved at 80 Volts, 10 sccm, 60 W microwave power, and 1.7 A extracted current. The total power consumption decreased with respect to input microwave power and gas flow rate; this held true for all bias voltages that were tested. This behavior may indicate that at higher flow rates (and higher gas pressures) the increase in electron-neutral collision frequency was responsible for an increase in total ionization rate. This is supported by Langmuir probe data, which shows an increase in plasma density as the flow rate is increased, at a fixed microwave power. The gas utilization, however, was best at low flow rates and high microwave power. At these conditions, there is more heating power deposited per neutral gas atom, which likely corresponds to a higher ionization fraction within the source. In general, for a given microwave power and flow rate, the total power consumption was roughly equal between the 80 V and 100 V bias tests, but was significantly higher in the 60 V bias test. Gas utilization increased with the bias voltage, since increasing the bias would cause a corresponding increase in current while holding the gas flow rate constant. These trends in the performance of the source will be investigated in more detail, in future work.

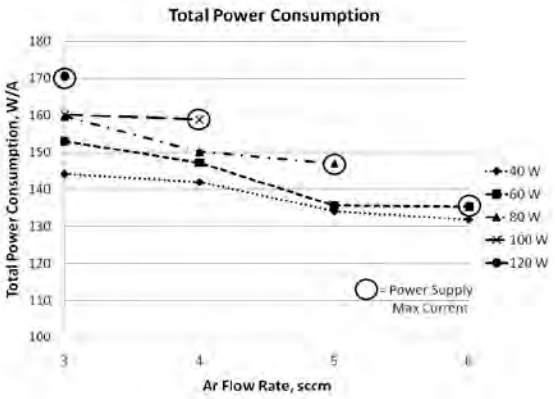

Figure 12. Total power consumed per Ampere. 4 mm extraction orifice, and 100 V bias.

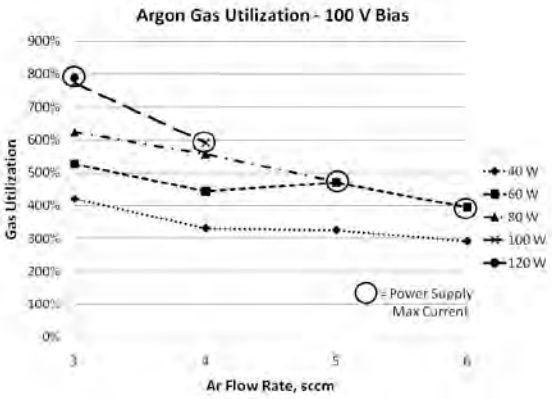

Figure 13. Feed gas utilization. 4 mm extraction orifice, and 100 V bias.

The gas utilization, defined as the extracted current divided by the equivalent current of neutral gas fed into the source, was plotted for the 100 V extraction case. The gas utilization data are shown in Fig. 13. Gas utilization factors of up to 790 percent, at 3 sccm, 120 W microwave power, and 1.7 A extracted current, were achieved. In all cases, the gas utilization was over 290 percent. It appears that there is a large amount of ion recycling within the source; that is, gas atoms are ionized within the source, the corresponding electron is extracted, the ion recombines at the wall of the source, and the process is repeated a few times on average for each ion. In this work, the recycling was a high as 8 times per ion, corresponding to basically 8 electrons per singly charged argon ion.

C. **Langmuir Probe Data**

In order to gain a better understanding of the plasma within the source with the 4 mm orifice during operation, a Langmuir probe was installed, near the exit plane of the source, and as close to the axis as possible. The probe tip was located 10 mm from the orifice plate, and roughly 11 mm from the centerline of the source. The extraction bias was fixed at 80 Volts, and probe traces were recorded at flow rates between 3 and 8 sccm, and microwave power levels from 40 to 100 W. The plasma density was calculated from the ion saturation current measured by the probe, and the results are shown in Fig. 14.

The densities recorded at the probe are significantly higher than the cutoff density for 2.45 GHz microwaves, which is 7.4×10^{10} cm^{-3}, so the plasma is overdense within the source. The plasma density appears to follow the same trends as the extracted current, as expected. In particular, the density increases with higher flow rates, which implies that the source may run even better at lower flow rates if the internal pressure can be increased.

The electron temperatures obtained from the probe traces are shown in Fig. 15. The trends in electron

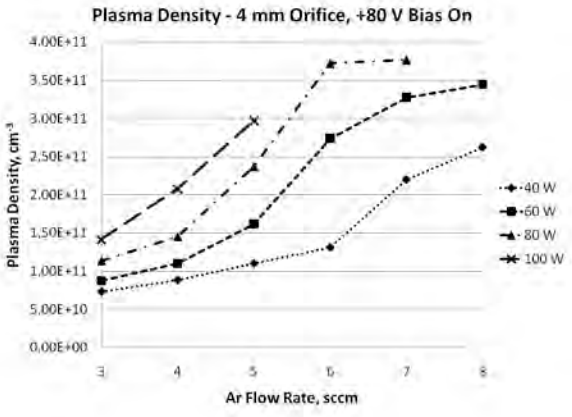

Figure 14. Plasma density from Langmuir probe traces. 4 mm extraction orifice, and 80 V bias.

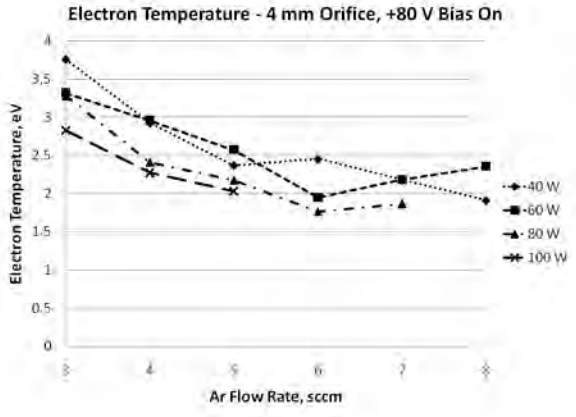

Figure 15. Electron temperature from Langmuir probe traces. 4 mm extraction orifice, 80 V bias.

temperature do not show anything unexpected for a low-temperature ECR plasma. Electron temperatures are in the 1.5 to 4 eV range. The temperature decreases slightly with increased flow rate, which is the result of increasing collision frequencies at higher pressures. With the plasma density and the electron temperature data, it is possible to estimate the amount of extractable current from the source, if a gross assumption of uniform plasma within the source is applied, by the formula,

$$I_e = A_{ori} \times \frac{1}{4} en \sqrt{\frac{8kT_e}{\pi m}} \tag{8}$$

where A_{ori} is the orifice cross-section area, n is the plasma density, T_e is the electron temperature, k is Boltzmann's constant, m is the electron mass, and e is the elementary charge. The measured electron currents were plotted against the calculated currents from the Langmuir probe data, and the results are shown in Fig. 16. There is a clear discrepancy between the measured current and calculated current; namely, the measured current is roughly 8 to 9 times higher than the expected current from the probe data. There are a few possible explanations for this. The plasma is not likely to be radially uniform, and may be higher near the orifice than it is at the probe. Also, the axial magnetic field lines facilitate electron flow directly from the ECR heating zone on axis to the orifice, which may be a factor. Finally, key to extraction is the shape of the plasma-facing sheath, which may account for the discrepancy. Another possible contributor to current would be electron beam driven ionization of the escaping gas in volume between the extractor plate and the orifice. Plasma measurements in this plume are left to future work, to gain a better understanding of the physics of source operation.

It is also worth noting that probe traces were taken with no bias applied to the extraction electrode, and the probe characteristics were not shaped like typical Langmuir probe traces. No electron saturation region appeared in the traces; in fact, very little electron current was collected at all. Electron currents collected at probe biases around 60 V were only on the order of tens of microamperes. Additionally, the ion currents continued to increase as the probe bias became more negative – the ion current did not saturate. It may be that when no voltage is applied, electrons are trapped within the strong magnetic field in the heating zone, and the magnetic field configuration acts as a magnetic nozzle within the source. This behavior is not well understood, and is still under investigation.

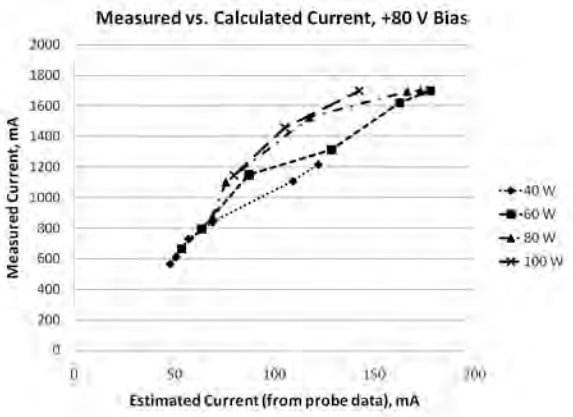

Figure 16. Measured current vs. expected current from Langmuir data.

D. **Performance Summary**

Based on this initial characterization of the U-M ECR waveguide plasma cathode, it appears that the device can deliver electron current with comparable levels of power consumption and gas utilization to many other plasma cathodes in the literature. The extracted currents recorded in this study were limited by the power supply unit, and based on the trends observed with respect to pressure, microwave power, and extraction voltage, it is reasonable to expect that some conditions may be able to deliver more than the 1.7 A currents reported here. The operating parameters corresponding to some of the better performance data are summarized in Table 1. The minimum amount of microwave heating power consumption and total power consumption are 32 W/A and 115 W/A, respectively. The maximum gas utilization factor that was achieved is 790 percent.

Table 1. Summary of plasma cathode performance.

	Max. Electron Current		Min. Heating Power Consumption	Min. Total Power Consumption	Max. Gas Utilization
Extracted Current [mA]	1700	1700	1259	1700	1700
Argon Flow Rate [sccm]	6	3	6	10	3
Absorbed Power [W]	60	120	40	60	120
Extraction Voltage [V]	100	100	100	80	100
Heating Power Consumption [W/A]	35	71	32	35	71
Total Power Consumption [W/A]	135	171	132	115	171
Argon Gas Utilization [%]	395	790	292	237	790

The performance of the U-M plasma cathode was plotted with several other sources from the literature, in Figs. 17 and 18. Figure 17 shows the heating power consumed per ampere of extracted current versus the gas flow rate. It should be pointed out that all of the comparison measurements in this study were performed with the source running on xenon, while all UM data was taken on argon. Substantial performance gains can be expected with xenon, owing to its larger mass and lower ionization potential. Although the comparison is not exactly perfect owing to gas differences, it does provide some insight into relative performance of the approaches investigated to date. There are three points included from the U-M source: one at minimum heating power consumption, one at minimum total power consumption, and one at maximum gas utilization. The U-M source consumes very little heating power when compared to other sources, but the flow rates required for these high efficiencies are higher than in other sources. In every test carried out on the U-M source, it appeared that higher pressure within the source would enhance the source performance. Operation on xenon would presumably reduce the flow requirement. One future test of the U-M source will involve decreasing the conductance of the extraction orifice further, to increase the source pressure at a fixed flow rate, or conversely, decreasing the required flow rate for a given operating pressure.

The total power consumption was plotted against gas flow rate for the various plasma cathodes, as shown in Fig. 18. The U-M source does not deliver the same relative efficiency in this case. But again, the UM source was operated on argon, due to cost considerations. Performance on

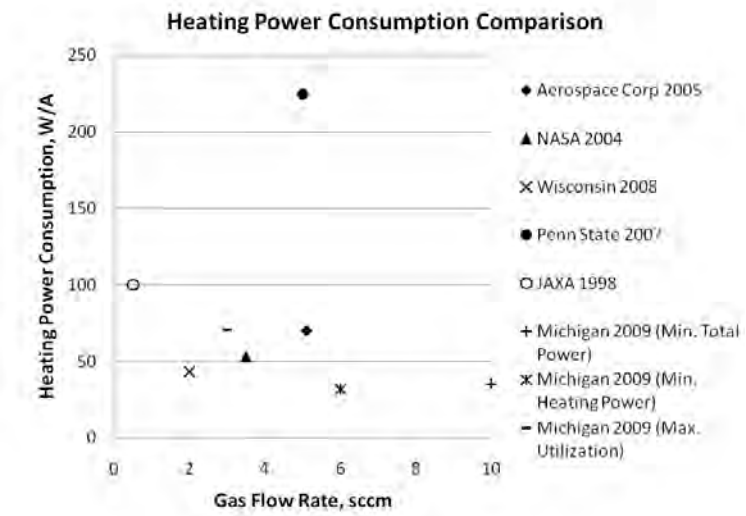

Figure 17. Heating power consumption versus flow rate, for several plasma cathodes in the literature.

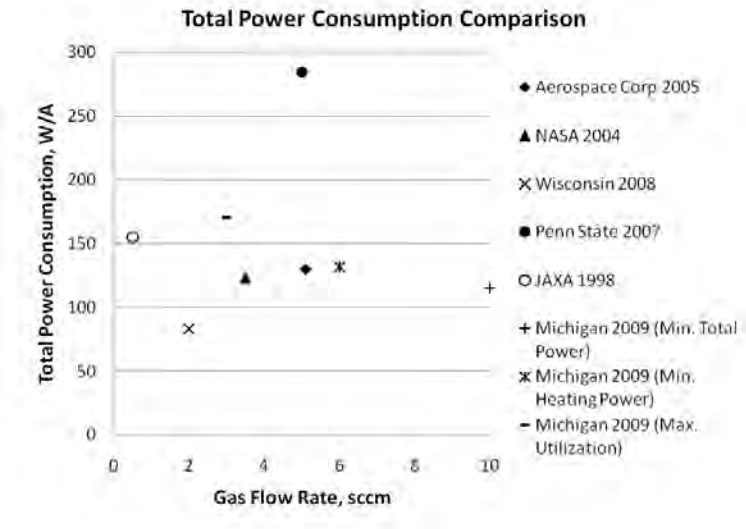

Figure 18. Total power consumption versus flow rate, for several plasma cathodes in the literature.

xenon is expected to lead to both a reduction in extraction voltage and required flow rates. Simple projections suggest that on xenon very high performance and efficiency should be within reach. The electron extraction geometry of the U-M source has yet to be optimized, so there is room for improvement on the total power efficiency. Future tests will include the development of a better extraction circuit, possibly including a keeper electrode, which may allow for comparable currents to be extracted at lower voltages, thereby reducing the total power consumption. In addition, the permanent magnet geometry is still unoptimized. Additional magnet rings can be added to the source to improve plasma uniformity and minimize electron losses to the source walls.

V. Conclusion

An ECR plasma cathode, based on a cylindrical waveguide design and using permanent magnets, has been designed for the main application of ion beam neutralization for those long-term missions where thermionic emitters would prove unsuitable. The available electron current from the source has been mapped out as a function of microwave power, extraction voltage, and argon flow rate. In addition, several extraction orifices were tested on the source, and the results show that the ECR source runs more efficiently at higher internal pressures. Langmuir probe data show unremarkable electron temperatures, and provide evidence of an overdense plasma within the source. The optimal power consumption and optimal gas utilization of the U-M source are comparable to those of other plasma cathodes in the literature. Future testing goals include the reduction of required flow rates and extraction voltages to achieve comparable extraction currents, increasing the source efficiency. Additionally, the maximum amount of available current from the source will be determined in the future, with the use of a power supply rated for higher currents, in order to avoid artificially limiting the extracted current.

Acknowledgments

Both authors thank NASA for funding this research through the Graduate Student Researchers Program (GSRP). Thanks to Dr. Hani Kamhawi at NASA Glenn Research Center for his extraordinary support.

References

[1]Rawlin, V.K., and Kerslake, W.R.," SERT II: Durability of the Hollow Cathode and Future Applications of Hollow Cathodes," J. Spacecraft, Vol. 7, No. 1, 1970.

[2]Sarver-Verhey, T.R., "Destructive Evaluation of a Xenon Hollow Cathode After a 28,000 Hour Life Test," *Proc.34th AIAA/ASME/SAE/ASEE Joint Propulsion Conference and Exhibit*, Cleveland, OH, July 13-15, 1998, AIAA Paper 2003-5279

[3]Sengupta, A., *et. al*, "An Overview of the Results from the 30,000 Hr Life Test of Deep Space 1 Flight Spare Ion Engine," *Proc.40th AIAA/ASME/SAE/ASEE Joint Propulsion Conference and Exhibit*, 11 - 14 July 2004, Fort Lauderdale, FL, AIAA Paper 2004-3812

[4]Vaughn, J., *et. al*, "NEXIS Reservoir Cathode 2000 Hour Proof-of-Concept Test," *Proc.40th AIAA/ASME/SAE/ASEE Joint Propulsion Conference and Exhibit*, 11 - 14 July 2004, Fort Lauderdale, FL, AIAA Paper 2004-4203

[5]Goebel, D., Watkins, R., and Jameson, K., "LaB_6 Hollow Cathodes for Ion and Hall Thrusters," *Journal of Propulsion and Power*, Vol. 23, No. 3, May–June 2007, pp. 552-558

[6]Hakayawa, Y., *et. al*, "Graphite Orificed Hollow Cathodes for Xenon Ion Thrusters," *Proc. 43rd AIAA/ASME/SAE/ASEE Joint Propulsion Conference and Exhibit*, 8-11 July, 2007, Cincinnati, OH, AIAA Paper 2007-5173

[7]Foster, J., "The High Power Electric Propulsion (HiPEP) Ion Thruster," *Proc. 40th AIAA/ASME/SAE/ASEE Joint Propulsion Conference and Exhibit*, 11 - 14 July 2004, Fort Lauderdale, FL, AIAA Paper 2004-3812

[7]Oks,E.M., "Physics and technique of plasma electron sources," *Plasma Sources Sci. and Technol.*, Vol. 1, 249, 1992

[9]Kuninaka, *et al.*, "Powered Flight of HAYABUSA in Deep Space," *Proc. 42nd AIAA/ASME/SAE/ASEE Joint Propulsion Conference and Exhibit*, 9-12 July, 2006, Sacramento, CA, AIAA Paper 2006-4318

[10]Kininaka, H. and Satori, S., "Development and Demonstration of a Cathodeless Electron Cyclotron Resonance Ion Thruster," *Journal of Propulsion and Power*, Vol. 14, No. 6, Nov-Dec. 1998, pp. 1022-1026

[11]Sang Wook-Kim, "Endurance Test of Microwave Engine," *Proc. 40th AIAA/ASME/SAE/ASEE Joint Propulsion Conference and Exhibit*, 11 - 14 July 2004, Fort Lauderdale, FL, AIAA Paper 2004-4126

[12]Diamant, K., "Resonant Cavity Hollow Cathode," *Proc. 41st AIAA/ASME/SAE/ASEE Joint Propulsion Conference and Exhibit*, 10-13 July, 2005, Tucson, AZ, AIAA Paper 2005-3662

[13]Edgar, M. C., and Bilén, S. G., "Design and Testing of a High Power Electron Cyclotron Resonance Neutralizer," *Proc. 43rd AIAA/ASME/SAE/ASEE Joint Propulsion Conference and Exhibit*, 8-11 July, 2007, Cincinnati, OH, AIAA Paper 2007-5289

[14]Kamhawi, H., Foster, J., and Patterson, M., "Operation of a Microwave Electron Cyclotron Resonance Cathode," *Proc. 40th AIAA/ASME/SAE/ASEE Joint Propulsion Conference and Exhibit*,11-14 July, 2004, Fort Lauderdale, FL, AIAA Paper 2004-3819

[15]Longmier, B. and Hershkowitz, N., "Improved Operation of the Nonambipolar Electron Source," *Rev. Sci. Instruments*, Vol. 79, Sept. 2008, 093506

[16]Weatherford, B. and Foster, J., "Characterization of a Waveguide ECR Plasma Source," *Proc. 44th AIAA/ASME/SAE/ASEE Joint Propulsion Conference and Exhibit*, 21-23 July, 2008, Hartford, CT, AIAA Paper 2008-4535